nature chemical biology

Enhancement of capillary leakage and restoration of lymphocyte egress by a chiral $S1P_1$ antagonist *in vivo*

M Germana Sanna[1,6], Sheng-Kai Wang[2,6], Pedro J Gonzalez-Cabrera[1,3], Anthony Don[1], David Marsolais[1], Melanie P Matheu[4], Sindy H Wei[4], Ian Parker[5], Euijung Jo[1], Wei-Chieh Cheng[2], Michael D Cahalan[4], Chi-Huey Wong[2] & Hugh Rosen[1]

Sphingosine 1-phosphate (S1P, 1) regulates vascular barrier and lymphoid development, as well as lymphocyte egress from lymphoid organs, by activating high-affinity $S1P_1$ receptors. We used reversible chemical probes (i) to gain mechanistic insights into S1P systems organization not accessible through genetic manipulations and (ii) to investigate their potential for therapeutic modulation. Vascular (but not airway) administration of the preferred *R* enantiomer of an *in vivo*–active chiral $S1P_1$ receptor antagonist induced loss of capillary integrity in mouse skin and lung. In contrast, the antagonist did not affect the number of constitutive blood lymphocytes. Instead, alteration of lymphocyte trafficking and phenotype required supraphysiological elevation of $S1P_1$ tone and was reversed by the antagonist. *In vivo* two-photon imaging of lymph nodes confirmed requirements for obligate agonism, and the data were consistent with the presence of a stromal barrier mechanism for gating lymphocyte egress. Thus, chemical modulation reveals differences in S1P-$S1P_1$ 'set points' among tissues and highlights both mechanistic advantages (lymphocyte sequestration) and risks (pulmonary edema) of therapeutic intervention.

Chemical agents provide powerful tools for dissecting complex physiological functions mediated through diverse receptor subtypes. In particular, selective agonist and antagonist pairs that are active *in vivo* have the distinct advantage of enabling acute, reversible modulation of molecular function while circumventing the developmental compensations that can arise in gene deletion studies. We have targeted this approach to the signaling pathway mediated by S1P and have thereby showed that *in vivo*–active reversible chemical tools can be used to address a series of mechanistic and therapeutic questions.

S1P is a pleiotropic autocrine and paracrine signaling lipid[1] that mediates graded rheostat control of numerous physiological functions through a family of G protein–coupled receptors. Small variations in ligand concentration are amplified by selective high-affinity receptors to acutely regulate vital functions such as heart rate[2,3], vascular and stromal barrier integrity[4] and lymphocyte egress[5]. The functioning of S1P receptors in the maintenance and modulation of biological barrier activity is of profound biological importance and has therapeutic implications[4], including prevention of transplant rejection and treatment of multiple sclerosis and perhaps adult respiratory distress syndrome as well[6].

Among the five known high-affinity S1P receptors, the $S1P_1$ receptor subtype is expressed by many cell types, including endothelial, blood and cardiac cells[1,6]. Genetic deletions of $S1P_1$ have revealed the receptor's essential endothelial functions in arterial smooth muscle cell migration; absence of $S1P_1$ results in embryonic lethality[7] and abnormalities in the development of the immune system[8,9]. These abnormalities relate both to cell egress from the thymus and to development of abnormal surface phenotypes such as elevated expression of the lymphocyte differentiation antigen CD69 (a retention signal for lymphoid egress[8,10–12]) on thymocytes and B cells. However, mechanistic interpretations derived from such gene deletion studies may be clouded by developmental compensations and anomalies.

Chemical approaches have also provided novel insights into the functioning of the S1P system. Reverse pharmacology using compounds of unknown molecular interaction that induce disappearance of lymphocytes from the blood and that proved to be S1P receptor agonists first identified the $S1P_1$ receptor as a target capable of inducing clinically useful immunosuppression[2,3,13]. Such agonists induce reversible inhibition of lymphocyte egress (known as lymphocyte sequestration) from the thymus, lymph nodes and Peyer's patch. Within 1 h of administration, nanomolar concentrations of agonists induce[14] and maintain immunosuppression[15,16] and promote maturation of late medullary thymocytes[14,17,18]. This observation, together with the organ and microanatomical selectivity of lymphocyte sequestration by agonists[13], led researchers to propose the existence of a stromal (endothelial) site for $S1P_1$ regulation of lymphocyte egress[5]. In support of this hypothesis, we showed in a recent two-photon imaging study of excised, perfused lymph node that agonist-dependent inhibition of lymphocyte trans-sinusoidal egress in the medulla is reversed

[1]Department of Immunology and The Scripps Research Institute Molecular Screening Center and [2]Department of Chemistry, The Scripps Research Institute, 10550 North Torrey Pines Road, La Jolla, California 92037, USA. [3]Genomics Institute of the Novartis Foundation, 10675 John Jay Hopkins Drive, San Diego, California 92121, USA. [4]Departments of Physiology and Biophysics and Center for Immunology and [5]Department of Neurobiology and Behavior, University of California, Irvine, California 92697, USA. [6]These authors contributed equally to this work. Correspondence should be addressed to H.R. (hrosen@scripps.edu) or C.-H.W. (wong@scripps.edu).

Received 13 February; accepted 8 June; published online 9 July 2006; doi:10.1038/nchembio804

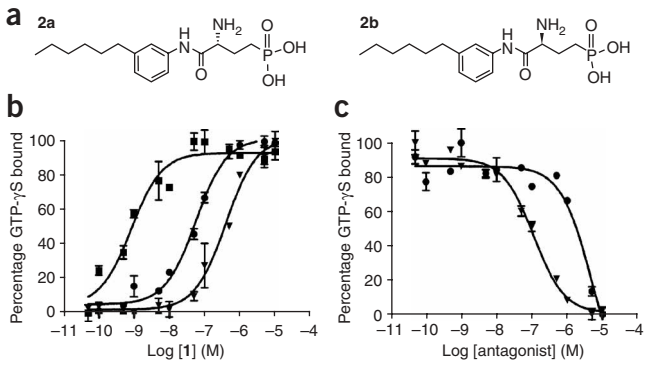

Figure 1 Compound **2a** is a selective antagonist for human $S1P_1$ ($hS1P_1$) receptor activation by the physiological agonist S1P. (**a**) Structures of **2a** and **2b**. (**b**) Shift in EC_{50} for S1P activation of $hS1P_1$ receptor by **2a** and **2b**. We tested CHO cell membranes expressing stably transfected $hS1P_1$ receptors for antagonism in a GTP-γS binding assay. Activation of $hS1P_1$ receptors by **1** alone (closed squares) or in the presence of 10 μM **2a** (inverted triangles) and **2b** (circles) is expressed normalized to percentage GTP-γS binding induced at maximal S1P concentration. The EC_{50} value was 0.8 nM for **1** alone; it was 398 nM and 50 nM in the presence of **2a** and **2b**, respectively. (**c**) We derived K_i values for S1P activation of the $hS1P_1$ receptor from antagonist competition curves; they were 77 nM for **2a** (inverted triangles) and 4.63 μM for **2b** (circles).

by antagonism[19]. In contrast, $S1P_1$ deletion studies have been interpreted as suggesting that agonists inhibit lymphocyte egress by 'functional antagonism', that is by causing a downregulation of lymphocyte-intrinsic $S1P_1$ receptors that mediate chemotaxis along an S1P gradient from node to lymph[8,9].

The complex multisystem biology through which S1P controls these diverse and essential functions via $S1P_1$ receptors is at present a topic of debate[1,20] and is best resolved *in vivo*. We have characterized selective, reversible chemical tools that acutely alter the set point of S1P-$S1P_1$ rheostats[21], and we have used them to discriminate between mechanisms that are controlled by basal, unperturbed levels of $S1P_1$ receptor-ligand tone and those that are induced by pathophysiologically or pharmacologically evoked excursions in S1P-$S1P_1$ occupancy and response. Here, we characterize a potent, selective, *in vivo*–active chiral antagonist of $S1P_1$ that inhibits both basal and induced S1P-$S1P_1$ responses. Using this antagonist in conjunction with a similarly effective, potency-matched, *in vivo*–active agonist[2,22], we are now able to acutely modulate $S1P_1$ activities that maintain vascular barrier function at physiological S1P concentrations in skin and lung capillaries, and we can also regulate the pharmacologically evoked $S1P_1$ agonism that is required for microanatomically selective lymphocyte sequestration in lymph nodes and for lymphocyte maturation in the thymic medulla.

RESULTS

Chiral $S1P_1$ antagonists with *in vivo* stability

Previously characterized antagonists of $S1P_1$ are limited by low potency[19], chemical lability[23], poor solubility and lack of *in vivo* activity. We hypothesized that replacing the phosphate ester with phosphonate could potentially create a potent and selective antagonist of $S1P_1$ having enhanced biological properties, provided that we paid careful attention to the chiral center and the head group (which has a double negative charge) as a prerequisite both for retention of potency in competition for S1P and for adequate formulation.

We synthesized the *R* (**2a**) and *S* (**2b**) enantiomers of 3-amino-4-(3-hexylphenylamino)-4-oxobutylphosphonic acid (**Fig. 1a**), which are useful competitive antagonists of $S1P_1$, to attempt to solve issues of selectivity, stability and (especially *in vivo*) efficacy. **2a** is a full competitive antagonist and is equipotent to the corresponding phosphate ester[23]. It shifted the effector concentration for half-maximum response (EC_{50}) for the physiological ligand **1** in a GTP-γS binding assay from 0.8 nM to 400 nM when in molar excess (**Fig. 1b**), with a K_i of ~70–80 nM (**Fig. 1c**). In contrast, the *S* enantiomer **2b** was less favored, having a K_i of 4.6 μM (**Fig. 1b**), and was therefore unlikely to have *in vivo* activity. We observed the same potency trend in competitive antagonism of the $S1P_1$-selective agonist SEW2871 (**3**; **Fig. 2a**)[2], that is **2a** (K_i of 18 nM) was substantially more potent than **2b** (K_i of 2.84 μM; **Fig. 2b**). The antagonistic effect of **2a** was selective for $S1P_1$ receptors, and **2a** showed neither agonism nor antagonism at 10 μM in GTP-γS assays for $S1P_2$, $S1P_3$ and $S1P_5$ receptors (data not shown; no data are available for $S1P_4$ receptors). These results are in contrast to those for antagonists that have an eight-member acyl chain, which showed strong antagonist activity on $S1P_3$ and $S1P_1$ receptors. **2a** was equipotent on mouse and human $S1P_1$ receptors, which share extracellular and transmembrane domain sequence identity.

In addition to competitively inhibiting receptor-proximal signaling events, such as G_i activation induced by **1** or **3** receptor binding, **2a** fully inhibited downstream events including ligand-induced receptor

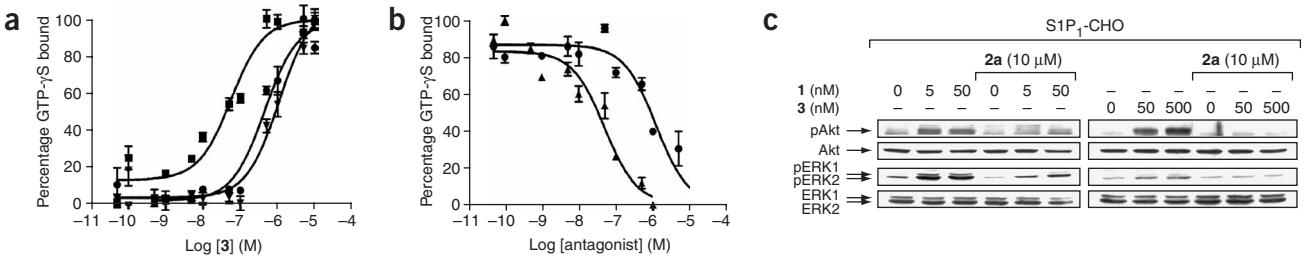

Figure 2 Compound **2a** is an antagonist for proximal and downstream signals from $hS1P_1$ receptor activation. (**a**) EC_{50} shift by **2a** and **2b** of **3** activation of $hS1P_1$ receptors. Curves show GTP-γS binding as a percentage of maximal responses induced by **3** for **3** alone (closed squares) and in the presence of S1P antagonists **2a** (1 μM; inverted triangles) and **2b** (10 μM; circles). EC_{50} values were 50 nM for **3** alone and 10 μM and 600 nM, respectively, in the presence of molar excess **2a** and **2b**. (**b**) K_i values for **3** activation of $hS1P_1$ receptors derived from antagonist competition curves for **2a** (inverted triangles) and **2b** (circles) were, respectively, 18 nM and 2.89 μM. (**c**) We serum starved CHO cells stably transfected with $S1P_1$ for 16 h, then we incubated them with **2a** at 10 μM for 1 h and stimulated them with either **1** or **3** at the indicated concentrations for 5 min. We performed western blot analyses of phospho-Akt, total Akt, phospho-ERK1/2 and total ERK1/2 levels as described in Methods ($n \geq 3$). Data are representative autoradiograms of one of three independent experiments. **2a** is a competitive inhibitor of Akt and ERK phosphorylation in response to $S1P_1$ activation by either **1** or **3**.

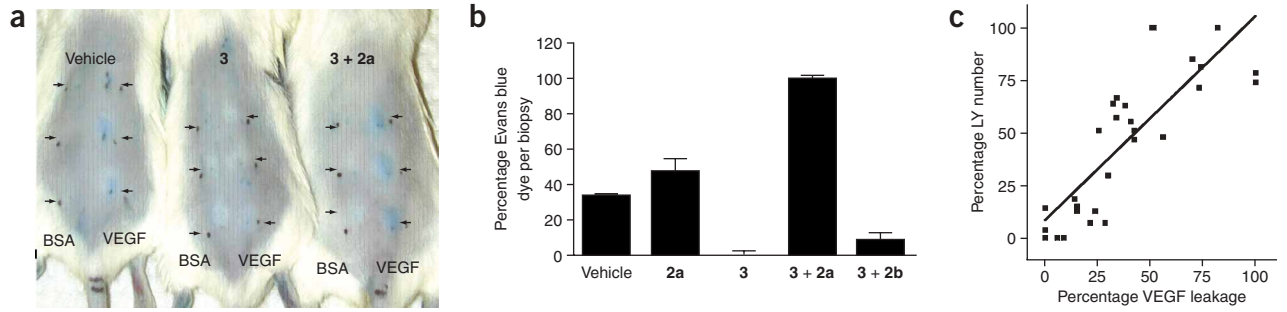

Figure 3 $S1P_1$ antagonism reverses protection from VEGF-induced leakage by the selective $S1P_1$ agonist **3**. (**a**) Representative photograph of the Miles assay in animals treated with $S1P_1$ agonist or antagonist. Skin leakage is visualized as the accumulation of blue dye. (**b**) Means of Evans blue dye leakage in biopsies (VEGF minus BSA) in treated animals from two pooled experiments. Error bars show ± 1 s.d. Statistical analyses were performed with ANOVA and the Bonferroni Multiple Comparisons Test. From left to right, n was 5, 5, 9, 11 and 3 mice for the respective groups. $P < 0.001$ for **3** versus vehicle or **2a**, and for **2a** versus **3** or the combination of **3** and **2b**. The S enantiomer **2b** failed to reverse protection by **3** from VEGF leakage. (**c**) Correlation between lymphopenia[13] and protection from VEGF-induced skin leakage across all treatment groups in **Figure 3b**. Scatter plot shows blood lymphocyte (LY) counts obtained in the experiments of **Figure 3b** against corresponding VEGF-induced skin leakage. Data are normalized to percentage of maximal leak or lymphopenia. A linear regression line is fitted to the data (slope is 0.97 ± 0.13; $r^2 = 0.67$).

internalization of green fluorescent protein (GFP)-tagged $S1P_1$ (**Supplementary Fig. 1** online). We also assessed the effect of **2a** on intracellular signals downstream of G protein activation that is dependent upon $S1P_1$ activation by measuring extracellular signal–regulated kinase (ERK) and Akt phosphorylation separately in response to S1P and the selective $S1P_1$ agonist **3** (**Fig. 2c**). **1** and **3** induction of the $S1P_1$-dependent accumulation of phospho-ERK and phospho-Akt were competitively inhibited by **2a**. We observed complete inhibition of the response to selective agonist **3** and >70% inhibition of responses to nonselective ligand **1**, results reflecting some basal expression of endogenous S1P receptors in the $S1P_1$-transfected Chinese hamster ovary (CHO) cell line. We saw no suppression of $S1P_3$-dependent ERK or Akt phosphorylation and no $S1P_3$ receptor agonism with **1** in CHO cells stably expressing $S1P_3$ (**Supplementary Fig. 2** online).

The phosphonate **2a** is more stable *in vivo* than its phosphate ester[23]. We could not detect the phosphate ester 5 min after intravenous injection in mice, whereas plasma concentrations of **2a** were 268 ± 98 nM at 5 h after a 10 mg kg^{-1} injection. We determined pharmacokinetic parameters of **2a** in cannulated rats ($n = 3$) by LC-MS and found a half-life of 73 ± 3 min, a small steady-state volume of distribution of 0.46 liter kg^{-1} and a modest plasma clearance of 4.63 ml min^{-1} kg^{-1}. We maintained an adequate *in vivo* receptor blockade for 5–6 h following a single injection of **2a**. We therefore evaluated the ability of this selective $S1P_1$ antagonist to alter vascular and lymphoid responses regulated by $S1P_1$ agonism under conditions of physiological $S1P_1$ tone and in the presence of an exogenous agonist.

$S1P_1$ antagonism enhances capillary leak

S1P agonism enhances endothelial barrier function in peripheral capillaries[24], lung[4,25] and lymphatic sinus[19] through cytoskeletal reorganization and changes to vascular endothelial cadherin junctions[26]. We found evidence for systemic blockade of $S1P_1$ receptors by **2a** (but not **2b**) within the vasculature for basal responses induced by both S1P and exogenous S1P agonists.

The target selectivity of **2a** was initially demonstrated by *in vivo* assessment of the reversal of effects evoked by the exogenous $S1P_1$-selective agonist **3** (ref. 2) and is illustrated in **Figure 3**. Administration of **3** (ref. 2) protected mice from vascular endothelial growth factor (VEGF)-induced skin leakage of Evans blue dye (complexed to plasma albumin) from plasma into the interstitial spaces (**Fig. 3a**), as quantified in skin-core biopsies and by dye extraction and spectrophotometric absorbance measurements (**Fig. 3b**). The preferred enantiomer **2a** entirely reversed the protective effects of **3** (**Fig. 3a,b**), whereas **2b** did not. Moreover, **2a** modestly enhanced skin capillary leakage in response to VEGF even when administered in

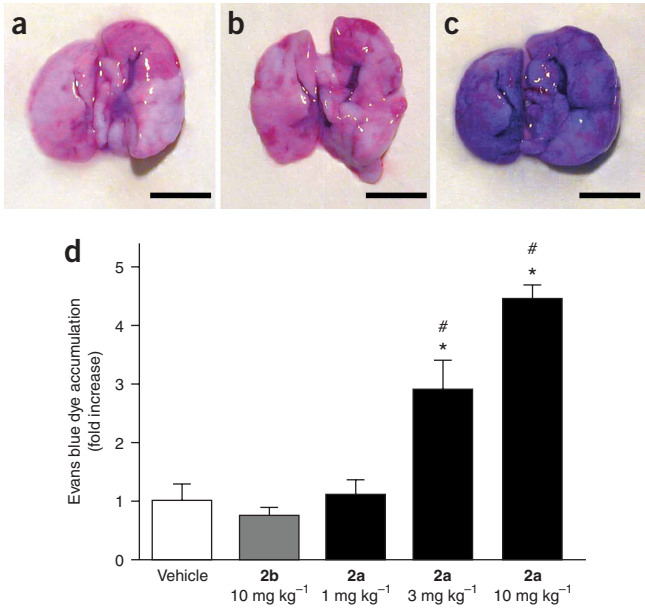

Figure 4 Basal $S1P_1$ tone provides protection from capillary leakage in lung. Systemic antagonism of $S1P_1$ under basal physiological conditions induced pulmonary leakage. Photographs show Evans blue dye accumulation in lungs 90 min after i.p. injection of either vehicle, **2b** (10 mg kg^{-1}) or **2a** (10 mg kg^{-1}). Histogram shows mean values of dye accumulation in the lungs of **2a**-treated C57BL1/6J mice, normalized to those of mice treated with vehicle alone. Bars indicate means ± s.d.; * indicates value is significantly different ($P < 0.05$) from vehicle; # indicates value is significantly different from **2b**. $n = 11$ for vehicle; $n = 3$ for **2a** at 1 and 3 mg kg^{-1}; $n = 9$ for **2b** and **2a** at 10 mg kg^{-1} as determined in three separate experiments for vehicle, **2b** and **2a** at 10 mg kg^{-1}.

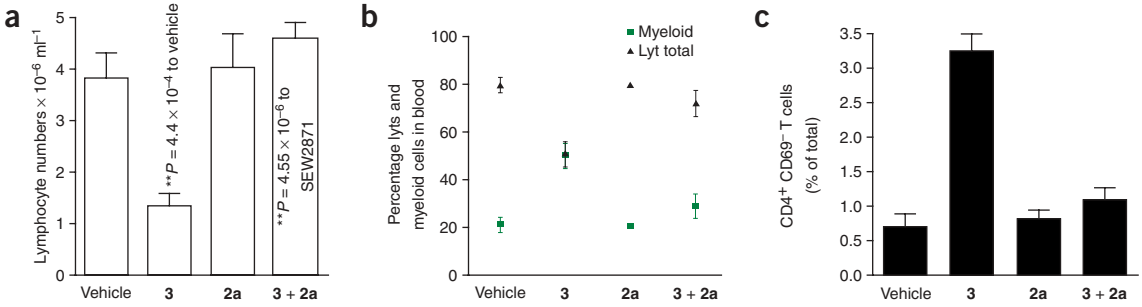

Figure 5 Systemic $S1P_1$ antagonism reverses agonist-induced sequestration of blood lymphocytes and medullary thymocyte phenotypic maturation. (**a**) The $S1P_1$ antagonist **2a** does not induce lymphopenia, and indeed it reverses agonist-induced lymphopenia. We administered **2a** (10 mg kg^{-1}) i.p. in C57BL6 mice at the time of oral dosing of **3** (20 mg kg^{-1}) or vehicle. We measured blood lymphocyte numbers as described[2] at 5 h. The data shown are pooled from four independent experiments with a total $n = 12$ mice per group. Mean ± s.d. and P values from Student's t-test are shown. (**b**) $S1P_1$ antagonist reverses agonist-induced alterations in differential leukocyte count (namely the percentage of lymphocytes, monocytes and neutrophils in the volume of blood counted) under the conditions and methods described in **Figure 5a**. Representative data ($n = 3$) from one of four similar experiments is shown. Because S1P agonists sequester lymphocytes (lyts) passing through specific lymphoid microenvironments, neutrophils and monocytes (myeloid cells) that do not traverse the same barriers are not sequestered. The number of myeloid cells remains constant while lymphocytes disappear, and therefore the percentage of myeloid cells rises. (**c**) $S1P_1$ antagonist reversal of agonist-induced loss of CD69 in late medullary thymocytes. We quantified CD69 expression on single-positive $CD4^+$ thymocytes by FACS at 5 h after administration of 20 mg kg^{-1} of **3** in the presence or absence of 10 mg kg^{-1} **2a**. Mean ± s.d., $n = 3$, data from one of two similar experiments is shown.

the absence of **3**, suggesting that endogenous $S1P_1$ tone contributes to the maintenance of basal capillary integrity.

$S1P_1$ blockade induces spontaneous pulmonary edema

To better evaluate the modulation of basal capillary integrity by endogenous S1P-$S1P_1$ tone, we sought an alternative model system in which a greater surface area of capillary endothelium exposed to plasma S1P could be assayed for permeability. This led us to study the lung by measuring leakage of Evans blue dye from the vasculature into the alveolar spaces[4]. The lung barrier consists solely of pulmonary microvascular endothelium and alveolar epithelial cells, each only one cell thick, separated by a thin extracellular matrix. The tight junctions between epithelial cells are impervious to the movement of small molecules, allowing the airway and vascular surfaces to be independently challenged with the antagonist.

Vascular administration of **2a** significantly enhanced basal pulmonary leakage by approximately 4.5-fold over vehicle ($P < 0.0001$) in a dose-dependent manner in the absence of any exogenous stimulus or ligand (**Fig. 4**), whereas **2b** was inactive. Pulmonary leakage was transient and clearance of **2a** from the plasma restored lung capillary integrity. Administration of $S1P_1$-selective agonist together with antagonist **2a** inhibited pulmonary leakage, confirming the mechanistic selectivity of pulmonary edema. Leakage is associated with loss of cortical actin organization within endothelial cells and is the subject of ongoing studies. In contrast to the effects of vascular administration, 75 μM **2a** did not induce measurable leakage on airway epithelial challenge. Thus, a basal level of vascular S1P-$S1P_1$ tone seems to be necessary to prevent pulmonary leakage, and this tone is disrupted by $S1P_1$ antagonism. The lack of activity of **2b** demonstrates the essential chirality for antagonist action and controls for the possibility of nonselective pulmonary leakage.

Reversal of agonist effects on lymphocyte egress and maturation

During the experiments in which we measured the effects of agonists and antagonists on capillary leak in response to VEGF administration, we obtained simultaneous counts of lymphocytes in peripheral blood to assess the loss of blood lymphocytes (lymphopenia) resulting from lymphocyte sequestration. A scatter plot (**Fig. 3c**) of the degree of vascular protection from VEGF leakage by $S1P_1$ agonism versus the induction of lymphopenia revealed a positive correlation between these parameters, both of which were reversed upon $S1P_1$ antagonism by **2a** (but not by **2b**). The selective $S1P_1$ agonist **3** induces reversible lymphocyte sequestration from peripheral blood with a time course matching the plasma half-life of the compound[2]. **3** induces neither a ligand-activated calcium response nor mitogen-activated protein (MAP) kinase phosphorylation in freshly isolated lymphocytes from spleen, lymph nodes or blood[2], but it has allowed the visualization of lymphocyte egress inhibition in lymph node explants and the demonstration of agonist-dependent stromal gating[19].

We found no significant alteration in either lymphocyte number (**Fig. 5a**) or percentage of lymphocytes within total white blood cell counts (differential count; **Fig. 5b**) after administration of **2a** alone in mouse peripheral blood. A single injection of 10 mg kg^{-1} of **2a** at the time of oral administration of **3** at doses up to 20 mg kg^{-1} abolished the agonist effects (**Fig. 5a**; $P \leq 4.5 \times 10^{-6}$), which alone was sufficient to induce and maintain lymphopenia for >24 h (ref. 2). **2b** was ineffective. Doses of **2a** as low as 3 mg kg^{-1} were sufficient to inhibit the lymphopenia induced by **3**.

We obtained further evidence that **2a** is able to maintain systemic inhibition of $S1P_1$ activation within lymphoid organs by measuring CD69 expression on single-positive $CD4^+$ thymocytes in thymic medulla. The well-characterized S1P agonists FTY720 (**4**)[17], its chiral analog AAL(R) (**5**)[14] and **3**[18] all induce rapid loss of CD69 immunoreactivity on these thymocytes, and flow cytometric analysis within 2 h of dosing reveals quantitative conversion of a CD69-intermediate population to $CD69^-$, a result that is likely to represent a lymphocyte-intrinsic effect of $S1P_1$ agonism. Analysis of $CD4^+$ single-positive thymocytes from mice treated with **3** and/or **2a** for 5 h showed that administration of **2a** alone has no effect on CD69 expression, whereas treatment with **3** induced an approximately sevenfold expansion of the $CD69^-$ $CD4^+$ single-positive population (**Fig. 5c**). This **3**-induced loss of CD69 was almost completely inhibited by **2a** pretreatment (**Fig. 5c**). **2a** therefore penetrates the matrix of lymphoid organs and inhibits effects (such as the rapid sequestration of lymphocytes in lymph nodes and Peyer's patch) attributable to activation of $S1P_1$ in both peripheral lymphoid systems and the thymus.

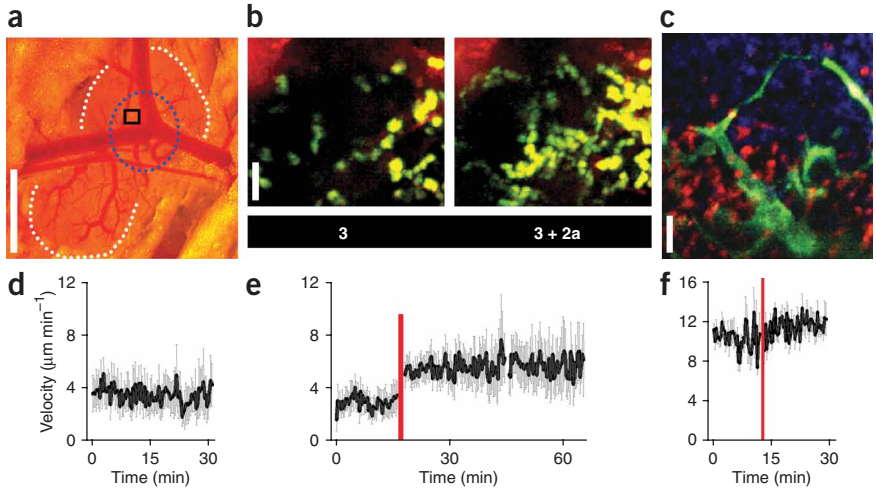

Figure 6 Imaging the *in vivo* kinetics of antagonist reversal of agonist-induced medullary arrest of T cells in inguinal lymph nodes by intravital two-photon fluorescence microscopy. (**a**) Inguinal lymph node of a BALB/c mouse with fat dissected away for multiphoton imaging. The node is outlined in white, the medullary region is circled in blue and a typical imaging frame is denoted by the black square. Scale bar, 1 mm. (**b**) Representative two-photon image of the medullary sinus of a **3**-treated mouse before antagonist injection and 18 min after antagonist injection. Carboxyfluorescein diacetate succinimidyl ester (CFSE)-labeled T cells are green; sinus tissue is red as described. Images show maximum intensity projections through a depth of 10 μm, and overlay images were captured at 28-second intervals for 8 min. The sinus space is outlined in white (scale bar, 20 μm). (**c**) Three-color image obtained in the cortical region, showing B cells (blue) in a follicle, T cells (red) and high endothelial venule (green); scale bar, 20 μm. (**d**) Instantaneous velocities (mean ± s.e.m.) of $CD4^+$ T cells in the medullary region 4 h after SEW2871 treatment. (**e**) Increase in medullary T-cell velocity after intravenous injection (red line) of 10 mg kg^{-1} of **2a** (**Supplementary Video 1**). Data are from the same imaging volume as in **Figure 6d**. (**f**) Velocity of $CD4^+$ T cells in the cortex of the lymph node 4 h after SEW2871 administration, before and after administration of **2a**, showing no alterations in cortical velocities.

In vivo two-photon imaging of antagonist effects in lymph nodes

We examined the dynamics of lymphocyte arrest and recovery by imaging, within an intravital (*in vivo*) preparation of the inguinal lymph node (**Fig. 6a**) of mice, the effects of a potency-matched combination of the agonist **3** and the antagonist **2a**. The procedures used for *in vivo* imaging of the inguinal lymph node (**Fig. 6a**) were previously described[27]. In addition, we defined landmarks for regional compartments within the medulla and cortex by *in vivo* staining using fluorescein isothiocyanate (FITC)-conjugated dextran to outline medullary sinuses (**Fig. 6b**) and blue-labeled B cells to identify B-cell follicles (**Fig. 6c**).

We administered agonist **3** before imaging to induce lymphocyte sequestration in the lymph nodes. We observed T lymphocytes arrested in the medullary region outside of empty sinuses (**Fig. 6b**) with velocities averaging only 3.5 μm min^{-1} (**Fig. 6d**). A time-lapse view of the sinus areas devoid of T lymphocytes is provided in

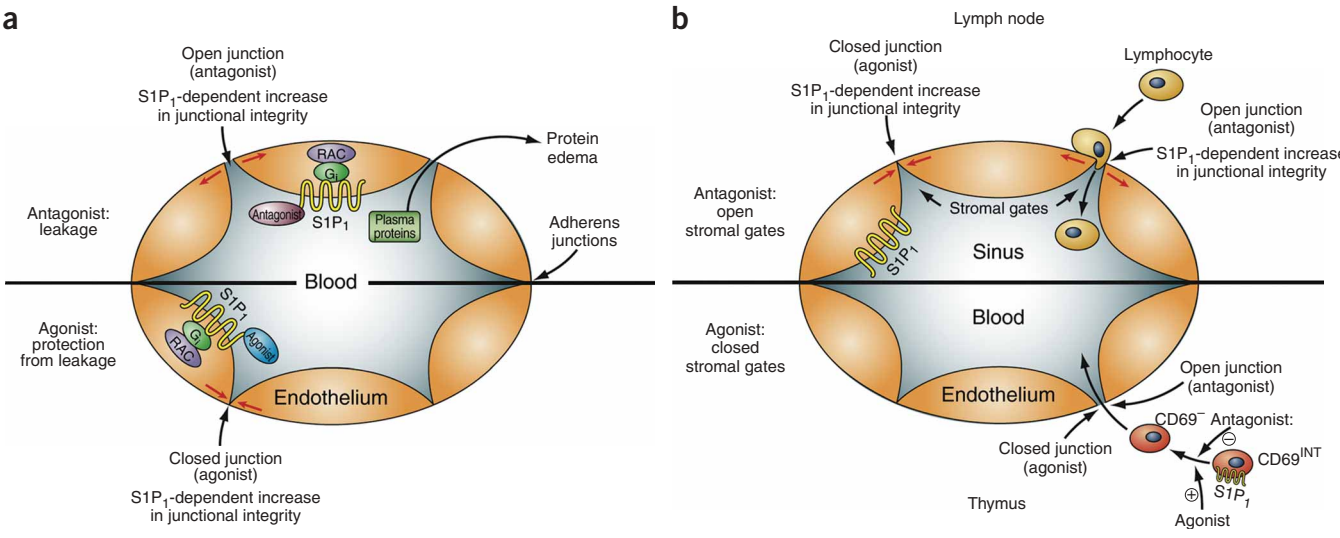

Figure 7 Models of the vascular and lymphoid effects of $S1P_1$ agonists and antagonists. (**a**) Agonism by the physiological ligand S1P (**1**) of endothelial cell $S1P_1$ receptors leads to the maintenance of adherens junctions[26] in both skin[24] and lung capillaries[25]. Alteration of endothelial junctional integrity by VEGF induces leakage of plasma proteins into interstitial spaces[24] and is reversed by pharmacologically selective $S1P_1$ agonist SEW2871. Competition for endogenous **1** activation of $S1P_1$ by **2a** induces plasma protein leakage in both skin capillaries and lung. (**b**) Lymphoid effects of $S1P_1$ antagonist **2a** are shown for lymph node (top) and thymus (bottom). Egress from both lymph node and thymus requires migration from basolateral to apical aspect of sinus lining or vascular endothelium in lymph node or thymus, respectively[5]; S1P agonists inhibit both processes and enhance organization of sinus endothelial junctions in lymph nodes[26]. Lymph node egress is maintained in the presence of **2a** alone, and also in the presence of physiological concentrations of S1P, and it is inhibited by pharmacological agonist **3** (ref. 2). Medullary lymphocyte arrest in nodes that is induced by **3** is reversed by antagonists[19], including **2a**. Blood lymphocyte numbers are maintained by **2a**, whereas agonist induces lymphopenia. In the thymus, **2a** prevents the CD69 intermediate $CD4^+$ or $CD8^+$ single-positive thymocyte downmodulation of the surface lectin and retention signal CD69 in response to agonist[14,18]. There is no direct evidence for $S1P_1$ regulation of thymic egress through thymic endothelium.

Supplementary Figure 3 online. Subsequent intravenous injection of **2a** induced a very rapid increase in average T-cell velocity to ~5.7 μm min^{-1} (**Fig. 6e**; **Supplementary Video 1** online), whereas control injections of vehicle had no effect (data not shown). In five out of six experiments, T-cell velocity in the medullary region recovered fully within 30 s (a single imaging time point) after intravenous administration of the antagonist (**Supplementary Video 1**; before and after videos of antagonist reversal of agonist arrest in lymph node medulla are shown in **Supplementary Video 2** online). T-cell velocities in these intravital experiments, measured in the presence of **3** alone or together with antagonist, correspond closely to values observed previously in an explant preparation[19]. In marked contrast to the effects in the medulla, corresponding measurements in the T-cell zone of the diffuse cortex showed no substantial changes in T-cell motility with either agonist or antagonist (**Fig. 6f**; **Supplementary Video 3** online). At the boundary between B-cell follicles and the T-cell zone, T cells maintained velocities of 10–11 μm min^{-1}, regardless of $S1P_1$ agonist or antagonist administration. Thus, agonist-induced lymphocyte arrest in the lymph node *in vivo* is restricted to the inhibition of medullary egress alone and is rapidly reversed in the presence of antagonist competition.

DISCUSSION

Here, we demonstrate that a selective chiral $S1P_1$ antagonist (**2a**) chosen for its distributional properties and stability *in vivo* can inhibit both basal and induced functions of the S1P-$S1P_1$ axis once adequately formulated. Unselected data derived from experiments in more than 120 mice show that **2a** has robust *in vivo* activity. We have confirmed the structure-activity relationships previously described[23], and it is notable that the intrinsic receptor binding potency is retained after conversion of the phosphate ester[23] to phosphonate. This observation suggests that the oxygen lone pair is not essential for receptor interactions. Acyl chain length contributes to selectivity: the octanyl analogs have strong antagonist activity toward both $S1P_1$ and $S1P_3$, and the hexanyl analogs are selective for $S1P_1$. The large difference in affinity between the *R* and *S* enantiomers points to a critical orientation of the head group in space, and this provides us with an *in vivo* inactive control that (excepting the head-group orientation) is chemically and physically identical to the active species. Moreover, the lack of biological actions of **2b** the *S* enantiomer, demonstrates that the effects of **2a** *in vivo* are related to its intrinsic receptor binding potency.

Regulation of vascular integrity by S1P

The systemic antagonism of $S1P_1$ receptors by **2a** evoked changes in vascular integrity under basal homeostatic (physiological) conditions and during pharmacological intervention. Protection of skin capillaries from VEGF-induced leakage by $S1P_1$ agonism was fully reversed by $S1P_1$ antagonism. Manipulation of the S1P-$S1P_1$ rheostat by pharmacological antagonism or agonism is of potential medical importance; for example, transient changes in the permeability of biological barriers, such as in the brain vasculature, may enhance delivery of drugs to otherwise inaccessible compartments. However, therapeutic attempts at antagonism need to be approached cautiously, as $S1P_1$ antagonism induces lung capillary leakage and may be implicated in renal reperfusion injury and cancer angiogenesis[28–30].

In the lung, we have shown that **2a** enhances leakage of marker dye under basal conditions when applied through the vasculature but not when applied via the airway. Thus, the constitutive integrity of the pulmonary capillary bed seems to depend on tonic plasma concentrations of S1P acting through $S1P_1$ receptors that are accessible exclusively from the vasculature. Furthermore, in conjunction with previous findings, these data illuminate the mechanism by which the spatial distribution of different S1P receptor subtypes having opposing actions to physiological ligands may function as a biological rheostat to regulate lung barrier function. Whereas we show here that $S1P_1$ agonism maintains capillary integrity and that antagonism breaches the pulmonary barrier, our earlier findings demonstrate that $S1P_3$ agonism on pulmonary epithelium causes dissolution of tight junctions *in vivo*, resulting in acute pulmonary edema[4]—an effect that is abolished by $S1P_3$ deletion.

By applying defined and selective chemical agonists (and now antagonists), in conjunction with genetic and compartmental approaches, to study the functions of S1P receptor subtypes, we have developed a model of the integrated spatial control of vascular physiology and pathology in the lung (**Fig. 7a**). Vascular S1P basal tone is likely to be important in protection from acute pulmonary edema and acute respiratory distress syndrome (ARDS) and may be an independent variable of potential use in determining the subset of patients susceptible to adult respiratory distress syndrome. Selective $S1P_1$ agonists therefore hold promise as therapeutic agents for enhancing lung barrier function as a treatment of pulmonary edema and ARDS[31–33].

$S1P_1$-receptor regulation of lymphocyte trafficking

Our *in vivo* studies using **2a** indicate that physiological S1P concentrations do not measurably alter constitutive lymphocyte recirculation, whereas pharmacological elevation in medullary $S1P_1$ tone by the S1P agonist **3** does induce lymphocyte sequestration (**Fig. 7b**). The critical role of pharmacological $S1P_1$ tone seems to be localized within the medulla of the lymph node, as evident from the rapid restoration of medullary T-cell motility and from the application of antagonist in the continued presence of agonist (**Fig. 6e**; **Supplementary Video 1**); by contrast, these agents were without effect, individually or together, in the cortical T-cell zone. Notably, **2a** applied alone caused no change in medullary T-cell movement or in blood lymphocyte numbers or expression of CD69 in thymic lymphocytes. However, it is effective in antagonizing (i) agonist-induced lymphopenia that is secondary to inhibition of lymphatic sinus egress[2,19] and (ii) $S1P_1$ agonist–induced phenotypic maturation (CD69 expression) of medullary thymocytes[14,18]. Thus, the homeostatic concentration of physiological S1P seems insufficient to modulate these functions, but they are affected by larger pharmacological deviations from the S1P-$S1P_1$ set point.

The actions of the specific antagonist **2a** aid in distinguishing between different mechanisms proposed to account for regulation of lymphocyte egress *in vivo* by $S1P_1$ receptors, namely intrinsic lymphocyte-receptor down modulation[8,34] versus stromal gating of lymphatic sinus barrier[1,19]. Extrapolations from $S1P_1$ gene deletion studies have been used to argue that chemical agonists work as 'functional antagonists' to cause downregulation of lymphocyte $S1P_1$ receptors that normally mediate chemotaxis out of the node and into the circulation along a gradient of S1P[8,35]. This model predicts that a systemic antagonist should mimic the actions of an agonist, resulting in sequestration of lymphocytes in the node. However, this was not apparent: only the agonist, but not antagonist, induced and maintained lymphopenia (**Fig. 5**). Thus, we conclude that a gradient of S1P-$S1P_1$ activation within lymphoid organs is not necessarily a point of regulation of constitutive egress[35], although we cannot rule out the possibility that a small, fractional priming signal in lymphocytes that is derived from small numbers of $S1P_1$ receptors is biologically relevant. Furthermore, neither $S1P_1$ agonists[14,18] nor $S1P_1$ antagonists replicate the developmental phenotypes of $S1P_1$ deletion (namely the

CD69 upregulation in single-positive medullary thymocytes seen in $S1P_1$-null lymphocytes[8]), and neither naive B cells nor naive T cells express CD69. Thus, acute sequestration of naive lymphocytes by $S1P_1$ agonists cannot be explained by functional antagonism of $S1P_1$ or by a direct interaction between CD69 and $S1P_1$ (ref. 12).

Observations of agonist-dependent sequestration of naive lymphocytes in Peyer's patch and lymph nodes, but not in splenic white pulp, suggest involvement of a stromal element functioning as a physical 'gate' to control lymphocyte trafficking over and above intrinsic lymphocytic mechanisms[5,13,36]. This mechanism is supported by two-photon microscopy in lymph node explants[19], which shows that lymphocyte movement across putative stromal 'portals' into lymphatic sinuses is constitutive and unaffected by an $S1P_1$-specific antagonist, ceases in the presence of $S1P_1$ agonist and recovers after addition of antagonist, observations consistent with the closing of stromal portals by the agonist. The intravital imaging data now presented, which show a system with fully intact vascular and lymphatic connections (**Fig. 6**), further validate this interpretation by replicating data for the actions of agonists on medullary (but not cortical) T-cell velocity loss and for antagonist-induced reversal and restoration of putative movement into sinus spaces, although we were unable to directly visualize trans-sinusoidal migration because *in vivo* labeling of the sinus barrier was not as clear as in the explant preparation.

Chemical biology of S1P signaling

$S1P_1$-mediated signaling provides a clear example of acute perturbations of biochemical activity through selective chemical approaches producing divergent results from gene deletion studies[1,18]. In another recent example[37], selective, functional chemical probes of granzymes A and B suggest a different hierarchy, and a distinct contribution of granzyme B to the biological mechanism of target-cell lysis by cytolytic T cells, from what had been deduced from prior gene deletion experiments. The possibility of developmental and compensatory changes following gene deletions complicates interpretation of results from such studies and requires that care be taken when extrapolating mechanisms from gene deletion studies to chemical biology and vice versa. However, a synergistic approach using both methodologies is likely to be profitable. Each interrogates different components of the integrated systems physiology by mechanisms that may turn out to be orthogonal.

The chemical tractability of the S1P-$S1P_1$ signaling axis presages rapid progress in therapeutic applications across immune, vascular and perhaps cancer biology. Potent, selective, reversible chemical probes of complex systems function, such as the $S1P_1$ antagonist and agonist combinations shown here, provide new, integrated insights into the organization and regulation of both the basal physiology and induced pathophysiology of such complex systems. Such probes also move fields forward across multiple disciplines by making highly reproducible experimental tools generally available.

METHODS

Chemical synthesis. The detailed synthetic route and full chemical characterization of **2a** and **2b** are shown in **Supplementary Methods** online.

S1P receptor agonists. We purchased **1** from BioMol and **3** (5-(4-phenyl-5-trifluoromethyl-thiophen-2-yl)-3-(3-trifluoromethyl-phenyl)-1,2,4-oxadiazole) from Maybridge.

Cell culture and transfection. D. Guerini (Novartis Pharma) provided CHO cells stably expressing human S1P receptors ($S1P_1$-CHO and $S1P_3$-CHO cells), and we maintained them in RPMI 1640 (Life Technologies, Gibco) containing 10% FBS, 0.5 mg ml^{-1} of the antibiotic G418, 50 μg ml^{-1} gentamicin, 100 units ml^{-1} penicillin, 100 μg ml^{-1} streptomycin and 10 mM HEPES. We transiently transfected the murine $S1P_1$ receptor provided by J. Chun in CHO cells as described[2].

Western blotting. We cultured control CHO cells and CHO cells stably transfected with human $S1P_1$ or $S1P_3$ to 50% confluence on six-well plates in complete RPMI 1640 supplemented with 10% FBS. We serum starved cells for 16 h and stimulated them with S1P or SEW2871 diluted to various concentrations in the serum-free medium with 0.1% fatty acid–free BSA. At 5 min, 1 h, or 4.5 h, we lysed cells in 50 mM Tris, pH 8.0, 125 mM NaCl, 20 mM CHAPS, 2 mM dithiothreitol, 1 mM EDTA, 2 mM Na_3VO_4, 10 mM NaF, 1 mM PMSF and protease inhibitor cocktail (Roche). We analyzed cell lysates by western blotting after separating them on 10% SDS-PAGE using mouse monoclonal antibody to phospho-ERK1/2 (sc-7383; Santa Cruz Biotechnology) and rabbit polyclonal antibody to phospho-Akt (BD Biosciences). We detected total ERK1 and ERK2 using a rabbit affinity-purified polyclonal antibody to ERK (sc-94; Santa Cruz Biotechnology), and we detected total Akt using a rabbit affinity-purified polyclonal antibody to Akt1 (BD Biosciences). We quantified band intensities corresponding to pERK1, pERK2 and pAkt by image analysis (Kodak 1D Scientific Imaging Systems), and we normalized amounts of pERK1/2 and pAkt for the total amounts of ERK1/2 and Akt.

Membrane preparation and receptor activation assay. We prepared membranes from CHO cells expressing human $S1P_1$, $S1P_2$, $S1P_3$ and $S1P_5$ for use in ligand and ^{35}S-GTP-γS binding studies as previously described[2]. For ^{35}S-GTP-γS binding assays, we added serial dilutions of **1** or **3** to membranes (1–10 μg protein per well) that were or were not preincubated for 30 min; we used the concentrations of **2a** and **2b** (and assayed them) as previously described[2].

Assays of capillary leakage. We assayed pulmonary leakage by measuring accumulation of plasma protein–bound Evans blue dye in the airways of lungs of C57BL1/6J mice treated with vehicle (**2a** or **2b**) that we solubilized according to previous descriptions[38]. We injected Evans blue dye intravenously 75 min after administering the compounds, and we perfused the lung vasculature to remove intravascular Evans blue dye before photography and dye quantification as described[4]. We performed the Miles assay[39] on the shaved dorsal skin of Balb/cByJ mice. We treated male mice weighing 30 g with vehicle (10 mM Na_2CO_3, 2% β-hydroxypropyl-cyclodextran) or **2a** (10 mg kg^{-1}) intraperitoneally (i.p.), and then we orally dosed them with **3** (20 mg kg^{-1}) or its vehicle. After 4.5 h, we injected the mice via the tail vein with 100 μl of a 0.5% Evans blue dye solution (Sigma) in saline. We then lightly anesthetized the mice with 2,2,2-tribromoethanol and adminstered murine VEGF165 (100 ng; Calbiochem) or vehicle (PBS in 0.1% BSA) by intradermal injection in triplicate in rows. We assessed the increase in vascular permeability 30 min later by measuring leakage of Evans blue dye into the injected site. After killing the mice, we biopsied the intradermal injection sites (3.5 mm, Sklar Tru-Punch) and incubated these in 100 μl of formamide at 58 °C to extract Evans blue dye. We read the absorbance of the extracts at 565 nm in a spectrophotometer.

Induction of lymphopenia in mice. We dosed C57BL6 mice orally with 10 mg kg^{-1} of **3** or vehicle (10% DMSO, 25% Tween20, v/v) and collected blood into EDTA tubes (Becton-Dickinson). We used a veterinary autoanalyzer calibrated for mouse blood (H2000, Careside) to make full blood counts at times stated previously[2]. All animal studies were approved by the Institutional Animal Care and Use Committee. We removed thymi as described and assayed the expression of CD69 on single-positive $CD4^+$ thymocytes by fluorescence flow cytometry as described[14,18].

Intravital imaging of lymphocyte migration by two-photon imaging. We performed adoptive transfer of $CD4^+$ T cells labeled with 5- and 6-carboxyfluorescein diacetate succinimidyl ester (Molecular Probes) as previously described[19,27] and analyzed the data as described[19]. We carried out microdissection to remove fat tissue that normally obscures the medullary region, and we performed imaging only in cases in which surrounding blood vessels were intact and rapid blood flow through large and small vessels could be seen under the light microscope. We visualized blood flow using video-rate two-photon imaging after intravenous injection of FITC-conjugated dextrans

(**Supplementary Video 1**). To stain the region of the medullary sinus, we injected dextrans conjugated with 20 kDa rhodamine into the footpad and skin of the ipsilateral flank after securing the imaging chamber and dissecting surrounding fatty tissue. In separate experiments, the rapid (5 min) appearance of fluorescent dextrans in the node after a single footpad injection confirmed that lymphatic circulation was intact. We anesthetized mice that had been orally treated with 10 mg kg^{-1} of **3** and imaged the inguinal lymph node between 4 and 6 h after dosing with **3**. We identified the medullary region using the large Y-shaped blood vessels overlaying the node as a landmark, and we performed medullary imaging out within 200 μm of the edge of the larger blood vessels. We obtained three-color images of the cortical region showing B cells in a follicle (labeled with 4-chloromethyl-6,8-difluoro-7-hydroxycoumarin, or CMF_2 HC), T cells (labeled with 5-(and-6)-(((4-chloromethyl)benzoyl)amino)-tetramethylrhodamine, or CMTMR) and high endothelial venule (labeled intravenously with 70 kDa FITC-conjugated dextran).

Plasma measurements and pharmacokinetics. We made plasma measurements in mice 5 h after i.p. injection of 10 mg kg^{-1} of **2a**, and we obtained detailed pharmacokinetic parameters after intravenous injection of 1 mg kg^{-1} of **2a** in cannulated rats ($n = 3$) as described in detail[9,10].

Statistical analysis. We performed all statistical analyses using GraphPad Prism 4 software, and we determined EC_{50} and K_i values by nonlinear regression and Schild analysis. We performed statistical analyses between groups of experimental animals using Anova and the Bonferroni Multiple Comparisons Test. We performed noncompartmental pharmacokinetic analysis of plasma levels using PK Solutions 2.0 software (Summit Research Services).

Note: Supplementary information is available on the Nature Chemical Biology website.

ACKNOWLEDGMENTS

We thank M. Cameron, L. Lin and P. Griffin for rat pharmacokinetics, B. Webb for LC-MS analysis of mouse plasma, X. Polk for GTP-γS assays, A. Chem for $S1P_2$ and $S1P_5$ GTP-γS assays, O. Safrina for T- and B-lymphocyte preparation and labeling and N. Gray and J. Isbell for access to the Chiralcel column. This work was supported by the National Institutes of Health (AI-055509 and NIMH-074404 to H.R., GM-41514 to M.D.C. and GM-48071 to I.P.). Work in the Rosen laboratory is also supported in part by a grant from Kyorin Pharmaceutical Company.

AUTHOR CONTRIBUTIONS

M.G.S., P.J.G.-C., A.D., D.M., E.J. and H.R. participated in the design and execution of the biological experiments. S.-K.W., W.-C.C. and C.-H.W. participated in the synthetic chemistry. M.P.M., S.H.W., I.P., M.D.C. and H.R. contributed to the design and execution of the multiphoton microscopy experiments. H.R., I.P., C.-H.W., M.D.C. and M.G.S. wrote the manuscript.

COMPETING INTERESTS STATEMENT

The authors declare that they have no competing financial interests.

Published online at http://www.nature.com/naturechemicalbiology
Reprints and permissions information is available online at http://npg.nature.com/reprintsandpermissions/

1. Rosen, H. & Goetzl, E.J. Sphingosine 1-phosphate and its receptors: an autocrine and paracrine network. *Nat. Rev. Immunol.* **5**, 560–570 (2005).
2. Sanna, M.G. *et al.* Sphingosine 1-phosphate (S1P) receptor subtypes S1P(1) and S1P(3), respectively, regulate lymphocyte recirculation and heart rate. *J. Biol. Chem.* **279**, 13839–13848 (2004).
3. Forrest, M. *et al.* Immune cell regulation and cardiovascular effects of sphingosine 1-phosphate receptor agonists in rodents are mediated via distinct receptor subtypes. *J. Pharmacol. Exp. Ther.* **309**, 758–768 (2004).
4. Gon, Y. *et al.* S1P3 receptor-induced reorganization of epithelial tight junctions compromises lung barrier integrity and is potentiated by TNF. *Proc. Natl. Acad. Sci. USA* **102**, 9270–9275 (2005).
5. Rosen, H., Sanna, M.G. & Alfonso, C. Egress: a receptor-regulated step in lymphocyte trafficking. *Immunol. Rev.* **195**, 160–177 (2003).
6. Goetzl, E.J. & Rosen, H. Regulation of immunity by lysosphingolipids and their G protein-coupled receptors. *J. Clin. Invest.* **114**, 1531–1537 (2004).
7. Liu, Y. *et al.* Edg-1, the G protein-coupled receptor for sphingosine-1-phosphate, is essential for vascular maturation. *J. Clin. Invest.* **106**, 951–961 (2000).
8. Matloubian, M. *et al.* Lymphocyte egress from thymus and peripheral lymphoid organs is dependent on S1P receptor 1. *Nature* **427**, 355–360 (2004).
9. Allende, M.L., Dreier, J.L., Mandala, S. & Proia, R.L. Expression of the Sphingosine 1-Phosphate Receptor, S1P1, on T-cells Controls Thymic Emigration. *J. Biol. Chem.* **279**, 15396–15401 (2004).
10. Nakayama, T. *et al.* The generation of mature, single-positive thymocytes in vivo is dysregulated by CD69 blockade or overexpression. *J. Immunol.* **168**, 87–94 (2002).
11. Feng, C. *et al.* A potential role for CD69 in thymocyte emigration. *Int. Immunol.* **14**, 535–544 (2002).
12. Shiow, L.R. *et al.* CD69 acts downstream of interferon-[alpha]/[beta] to inhibit S1P1 and lymphocyte egress from lymphoid organs. *Nature* **440**, 540–544 (2006).
13. Mandala, S. *et al.* Alteration of lymphocyte trafficking by sphingosine-1-phosphate receptor agonists. *Science* **296**, 346–349 (2002).
14. Rosen, H., Alfonso, C., Surh, C.D. & McHeyzer-Williams, M.G. Rapid induction of medullary thymocyte phenotypic maturation and egress inhibition by nanomolar sphingosine 1-phosphate receptor agonist. *Proc. Natl. Acad. Sci. USA* **100**, 10907–10912 (2003).
15. Budde, K. *et al.* Pharmacodynamics of single doses of the novel immunosuppressant FTY720 in stable renal transplant patients. *Am. J. Transplant.* **3**, 846–854 (2003).
16. Budde, K. *et al.* First human trial of FTY720, a novel immunomodulator, in stable renal transplant patients. *J. Am. Soc. Nephrol.* **13**, 1073–1083 (2002).
17. Yagi, H. *et al.* Immunosuppressant FTY720 inhibits thymocyte emigration. *Eur. J. Immunol.* **30**, 1435–1444 (2000).
18. Alfonso, C., McHeyzer-Williams, M. & Rosen, H. CD69 down-modulation and inhibition of thymic egress by short and long-term selective chemical agonism of S1P1 receptors. *Eur. J. Immunol.* **36**, 149–159 (2006).
19. Wei, S.H. *et al.* Sphingosine 1-phosphate type 1 receptor agonism inhibits transendothelial migration of medullary T cells to lymphatic sinuses. *Nat. Immunol.* **6**, 1228–1235 (2005).
20. Ley, K. & Morris, M. Signals for lymphocyte egress. *Nat. Immunol.* **6**, 1215–1216 (2005).
21. Spiegel, S. & Milstien, M. Sphingosine 1-phosphate: an enigmatic signalling lipid. *Nat. Rev. Mol. Cell Biol.* **4**, 397–407 (2003).
22. Jo, E. *et al.* S1P1-selective in vivo-active agonists from high-throughput screening: off-the-shelf chemical probes of receptor interactions, signaling, and fate. *Chem. Biol.* **12**, 703–715 (2005).
23. Davis, M.D., Clemens, J.J., Macdonald, T.L. & Lynch, K.R. Sphingosine 1-phosphate analogs as receptor antagonists. *J. Biol. Chem.* **280**, 9833–9841 (2005).
24. Sanchez, T. *et al.* Phosphorylation and action of the immunomodulator FTY720 inhibits VEGF-induced vascular permeability. *J. Biol. Chem.* **278**, 47281–47290 (2003).
25. McVerry, B. *et al.* Sphingosine 1-phosphate reduces vascular leak in murine and canine models of acute lung injury. *Am. J. Respir. Crit. Care Med.* **170**, 987–993 (2004).
26. Singer, I.I. *et al.* Sphingosine-1-phosphate agonists increase macrophage homing, lymphocyte contacts, and endothelial junctional complex formation in murine lymph nodes. *J. Immunol.* **175**, 7151–7161 (2005).
27. Miller, M.J., Wei, S.H., Cahalan, M.D. & Parker, I. Autonomous T cell trafficking examined in vivo with intravital two-photon microscopy. *Proc. Natl. Acad. Sci. USA* **100**, 2604–2609 (2003).
28. Awad, A.S. *et al.* Selective sphingosine 1-phosphate 1 (S1P1) receptor activation reduces ischemia-reperfusion injury in mouse kidney. *Am. J. Physiol. Renal. Physiol.* **290**, F1516–F1524(2006).
29. Ho, J.W.Y. *et al.* Effects of a novel immunomodulating agent, FTY720, on tumor growth and angiogenesis in hepatocellular carcinoma. *Mol. Cancer Ther.* **4**, 1430–1438 (2005).
30. LaMontagne, K. *et al.* Antagonism of sphingosine-1-phosphate receptors by FTY720 inhibits angiogenesis and tumor vascularization. *Cancer Res.* **66**, 221–231 (2006).
31. McVerry, B. & Garcia, J. In vitro and in vivo modulation of vascular barrier integrity by sphingosine 1-phosphate: mechanistic insights. *Cell. Signal.* **17**, 131–139 (2005).
32. Garcia, J.G.N. *et al.* Sphingosine 1-phosphate promotes endothelial cell barrier integrity by Edg-dependent cytoskeletal rearrangement. *J. Clin. Invest.* **108**, 689–701 (2001).
33. McVerry, B. & Garcia, J. Endothelial cell barrier regulation by sphingosine 1-phosphate. *J. Cell. Biochem.* **92**, 1075–1085 (2004).
34. Graeler, M., Shankar, G. & Goetzl, E. Cutting edge: suppression of T cell chemotaxis by sphingosine 1-phosphate. *J. Immunol.* **169**, 4084–4087 (2002).
35. Lo, C., Xu, Y., Proia, R. & Cyster, J. Cyclical modulation of sphingosine-1-phosphate receptor 1 surface expression during lymphocyte recirculation and relationship to lymphoid organ transit. *J. Exp. Med.* **201**, 291–301 (2005).
36. Rosen, H. & Liao, J.Y. Sphingosine 1-phosphate pathway therapeutics: a lipid ligand-receptor paradigm. *Curr. Opin. Chem. Biol.* **7**, 461–468 (2003).
37. Mahrus, S. & Craik, C.S. Selective chemical functional probes of granzymes A and B reveal granzyme B is a major effector of natural killer cell-mediated lysis of target cells. *Chem. Biol.* **12**, 567–577 (2005).
38. Hale, J.J. *et al.* Potent S1P receptor agonists replicate the pharmacologic actions of the novel immune modulator FTY720. *Bioorg. Med. Chem. Lett.* **14**, 3351–3355 (2004).
39. Miles, A. & Miles, E. Vascular reactions to histamine, histamine liberators or leukotoxins in the skin of the guinea pig. *J. Physiol. (Lond.)* **118**, 228–257 (1952).